Approach to Heterogeneous Strain Distribution in Cable-In-Conduit Conductors Through Finite Element Simulation

H. Bajas, D. Durville, D. Ciazynski, and A. Devred

***Abstract*—The ITER Cable-In-Conduit Conductors are submitted to high thermal and electromagnetic cyclic loadings responsible for conductivity loss in the strain-sensitive Nb_3Sn strands. The complex mechanical phenomena occurring at the local scale of the strands make the final performances of the CICC difficult to predict from single-strand properties. In order to assess the amplitudes of the local strains that drive the conductor electrical behavior, a nonlinear finite element simulation code is used. The successive stages of the conductors' service life, from the forming of the cable to its thermal cool down and Lorentz force loading, are simulated. Each strand is individually modeled along with the great number of contacts-friction interactions between the strands. This paper presents the simulation results obtained for 144 strand cables of two different designs. It is shown that the various loadings result in a heterogeneous distribution of strains along and across the strands with occurrence of extreme tensions and compressions. The use of simulation would eventually help to better characterize the influence of conductor design parameters.**

***Index Terms*—Axial strain, bending, cable mechanics, CICC, damages, finite element simulation, ITER, Nb_3Sn degradation.**

I. Introduction

THE ITER Cable-In-Conduit Conductors (CICCs) are made of an assembly of Nb_3Sn-based strands and pure copper wires cabled together and inserted in a stainless steel jacket. During the cool down of the conductor from heat treatment to operating temperature, the cable is submitted to a thermal compression induced by the differential of thermal contraction between the Nb_3Sn and the jacket. In addition, the local Lorentz force loadings induced by the combination of current and external magnetic field yield to additional stresses applied to the strands [1], [2]. Both loadings cause the occurrence of strains at the local scale in Nb_3Sn filaments that degrade their current-carrying capacity. The sensitivity of the brittle Nb_3Sn material to strain in terms of conductivity loss is well established for single strand by the TARSIS experiment and supported by microscopic observations of filament crack initiation [3], [4]. However, what are the amplitudes of the strains locally sustained by the filaments in a loaded cable is not clear and predicting the performances of CICC remains an issue [5]–[7]. In the past few years, some numerical models of cable have attempted to address this problem using various classic FE packages with 3D linear solid elements or beam and shell elements [12], [13]. The problem is then solved using either explicit or implicit resolution methods. But the prediction of the contact positions between large numbers of elements is still an important issue for these models along with convergence trouble due to the numerous non-linearities of the problem. Several difficulties are also faced regarding the boundary conditions at the strands ends or the simulation of the final compaction of the cable. Now, a dedicated finite element code, initially developed for the modelling of entangled media [9], [10] has been adapted to consider the layout and the specific loadings of CICCs in order to assess the local strains along each individual strand. Details about these developments can be found in [11]. The simulation starts with the computation of a relevant cable geometry by modeling the conductor manufacturing, before applying a thermal compression and an electromagnetic loading.

H. Bajas and D. Durville are with the Laboratoire MSSMat, Ecole Centrale Paris/CNRS UMR8579, Grande Voie des Vignes, 92295 Chatenay-Malabry Cedex, France (e-mail: hugues.bajas@ecp.fr; damien.durville@ecp.fr).

D. Ciazynski is with the Association Euratom-CEA, CEA/DSM/DRFC, Centre de Cadarache, 13108 Saint-Paul-Lez-Durance, France (e-mail: daniel.ciazynski@cea.fr).

E. Devred is with the ITER Organization, Cadarache, 13108 Saint-Paul-Lez-Durance, France (e-mail: Arnaud.Devred@iter.org).

II. Finite Element Model Main Features

The developed simulation code determines the mechanical equilibrium of assemblies of fibers or wires submitted to large transformations, taking into account of contact-friction interactions between fibers, under quasi-static assumptions and using an implicit solution scheme. A kinematically enriched finite strain beam model, describing the kinematics of each cross-section by means of a vector position for its center and two unconstrained directors, thus allowing the consideration of planar deformations of these cross-sections, is used to represent the behavior of individual wires in the cable. The full three dimensional strain tensor derived from this formulation allows a 3D orthotropic elasto-plastic constitutive law to be employed, with a yield criterion depending only on the axial strain in the wire. Cyclic irreversible plastic effects occurring in the axial direction of strands can then be taken into account. In addition to the issues related to the nonlinear solving of contact-friction interactions, the determination of proper boundary conditions to be applied at the ends of the simulated sample is one of the main difficulties of the problem. Special pseudo-periodic conditions

linking displacements at both ends of the sample have been developed for this purpose [11].

III. Simulation of Conductors

A. Shaping of the Cable

The trajectories of the strands inside a CICC are not known *a priori* and thus need to be calculated. Since the number of strands considered by the code is limited for reasons of computational cost, only one petal of the full size conductor is considered. The geometry of compacted cable is computed during the shaping process of the simulation. An initial theoretical configuration of wires is described as helices recursively defined on helices which represent the different stages of the cable and is then deformed by two planes and two cylindrical tools. These rigid tools prescribe their displacements to gradually compact the assembly until a desired void fraction. The shaping is performed considering an elastic behavior. The consideration of an orthotropic constitutive law just at the end of the shaping, allows the irreversible plastic transverse pinching of wires to be modeled. The effect of the heat treatment is then simulated by resetting the induced residual stresses.

After the cable shaping, the material properties are switched to the elasto-plastic model with appropriate constitutive laws for the Nb_3Sn strand and the copper wire identified in axial and transverse direction from experimental data [3], [11]. Details on the elasto-plastic model are presented in [11]. The friction coefficient between strands is taken equal to 0.25. Friction between jacket and cable is also considered but only concerns the transverse displacements (no longitudinal friction effect). The geometry of cable and its mechanical behavior have been earlier validated in the axial and transverse directions for 36- and 45-strand conductors [11], [14].

B. Thermal Cool Down

In order to simulate the thermal effects, the shaped cable is compressed in its axial direction by prescribing identical axial displacement to each strand ends. The cable is compressed up to -0.67% according to admitted results from [2], [5].

C. Lorentz Force Loading

The Lorentz force loading is simulated by the application of lineic loads applied along the strands. These loads are applied only to the superconducting strands and are oriented in a transverse direction (not orthogonally to the strands). The model assumes uniformly distributed current among the strands and the local forces are taken equal everywhere in the cable. The Lorentz force per strand is taken equal to 0.84 N/m that would correspond to a current per strand of 76 A in a field of 11 T.

IV. Simulation Results and Discussion

A. Models of Conductors

The different features of the code are now used to simulate two conductors made of 144 strands with one third of pure copper wires and two thirds of superconducting strands with the following cabling pattern: $(2\,\mathrm{sc.} + 1\,\mathrm{cu.}) \times 3 \times 4 \times 4$. The length of the samples is 300 mm and the diameter of the strands is 0.82 mm. The two cables only differ from their void fractions and their twist pitches sequences. The first cable referred to as *Option I* sample has a large void fraction and short twist pitches compared to *Option II* sample (Table I). The initial configuration of the conductor with the tools and the result of the shaping for the *Option I* sample are shown in Fig. 1.

TABLE I
Model of Conductors

	Option I sample	Option II sample
Cable pattern	(2 sc. + 1cu.) x 3 x 4 x 4	
Void fraction [%]	35	29
Twist pitches [mm]	45 - 85 - 125 - 250	80 – 140 – 190 - 300

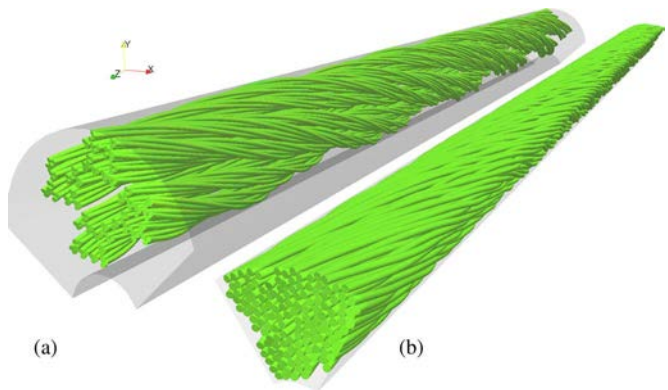

Fig. 1. Views of the 144 strand petal conductor with the tools. (a) Initial and (b) final configurations.

B. High Heterogeneity of the Axial Strains

In response to the axial compression and the Lorentz force loading, the simulation shows different behaviors for the two samples. Different distributions of local axial strains develop in the strands of the two cables (Figs. 2 and 3). From these figures, the "conductors' strain states appear" to be highly heterogeneous with important variations of strains along and across the strands and different bending orientations. Some high compressions are visible on the upper part of the *Option I* sample in the direction of the Lorentz force loading in Fig. 2(a). More buckling appears in the *Option II* sample with more pronounced effect at the cable ends in Fig. 2(b), likely due to lack of precision from the boundary conditions.

The model illustrates that the applied thermal compression induces simultaneously both pure compression and bending of the strands that take advantage of the free space around them to move [5], [11], [14]. The great variety of possible strains found within the conductor is illustrated by the broadness of the axial strain distributions in Fig. 4. On this plot, the axial strains are relative to the Nb_3Sn filament region (of a diameter of 0.622 mm) for only the superconducting strands. The mean strain value in the strands significantly differs from the global strain of -0.67% (Table II) The Lorentz force loading tends to increase the compression as the shift of the distribution to high compressive strains and its broadening tends to show (Fig. 4).

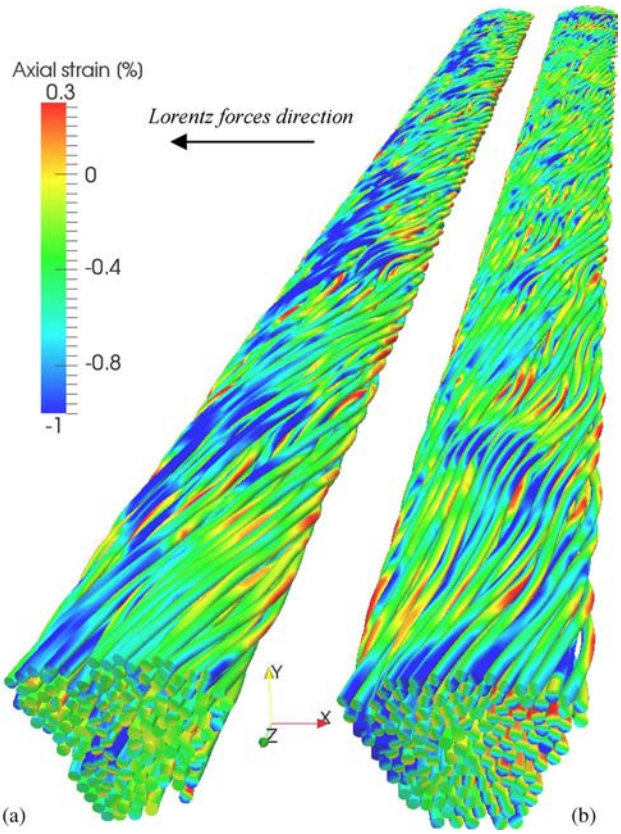

Fig. 2. Views of the 144 strand petal for (a) Option I and (b) Option II conductors. Strain state after axial compression and Lorentz force loading. The values range from −1 to 0.3% to enhance the contrast.

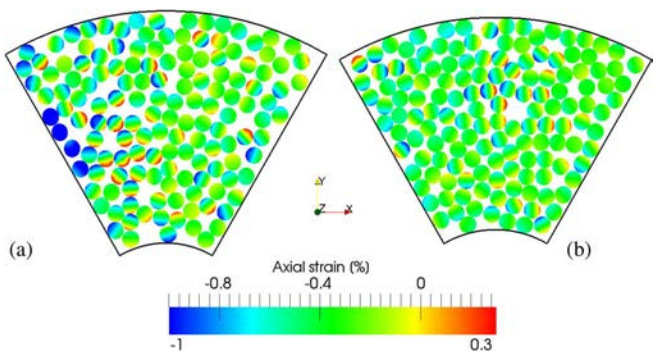

Fig. 3. Views of the cross-sections of the conductors after Lorentz force loading for (a) short pitches and 35% void fraction and (b) long pitches and 29% void fraction.

The axial strains predicted by the model range from −1.8% to +0.8% with broad distributions of intermediate values.

The simulation demonstrates that the combination of pure compression and bending of the strands results in a heterogeneous distribution of axial strains that questions some of the previously accepted assumptions [2], [6], [8] about uniformly distributed strains.

C. Importance of the Critical Strain Values

As previously reported in [11], [19]–[21], due to the local bending, some of the strains largely differ from the mean value.

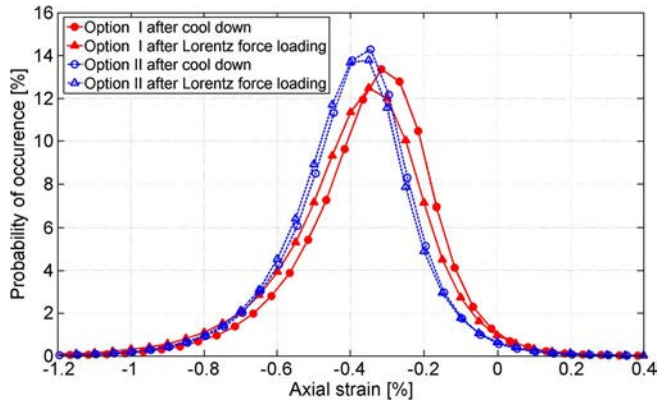

Fig. 4. Axial strains distributions relative to the filamentary region of the superconducting strands for the two samples after and before Lorentz force loading.

TABLE II
AXIAL STRAIN STATISTICS

	After cool down	After Lorentz loading
Option I sample		
Mean axial strain	0.351 %	0.386 %
% of values > +0.3 %	0.0354 %	0.0529 %
% of values < -0.8 %	1.85 %	3.29 %
Option II sample		
Mean axial strain	-0.396 %	-0.404%
% of values > +0.3 %	0.0492 %	0.0561 %
% of values < -0.8 %	2.14%	2.24 %

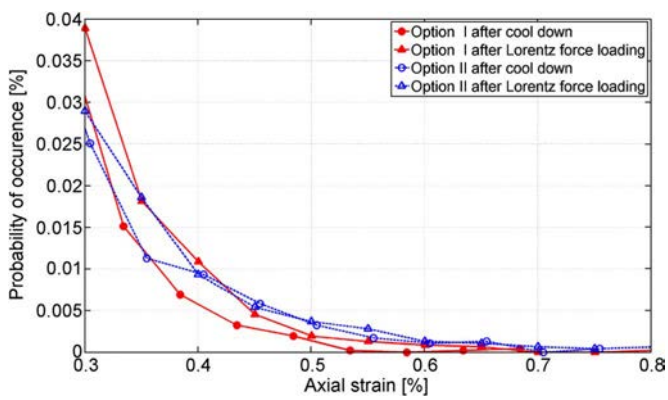

Fig. 5. Tails of the distributions for the tensile part for the two tested samples before and after Lorentz force loading.

The occurrence of critical strains that may occur in the filamentary region is highlighted by the tails of the distributions. In Fig. 5, the tensile part extends up to a domain where Nb_3Sn filaments might be damaged [16], [17]. In Fig. 6, the compressive part reaches a domain where the critical current of the Nb_3Sn is close to zero [18]. The low proportion of critical events in Table II reflects the occurrence of very localized situations.

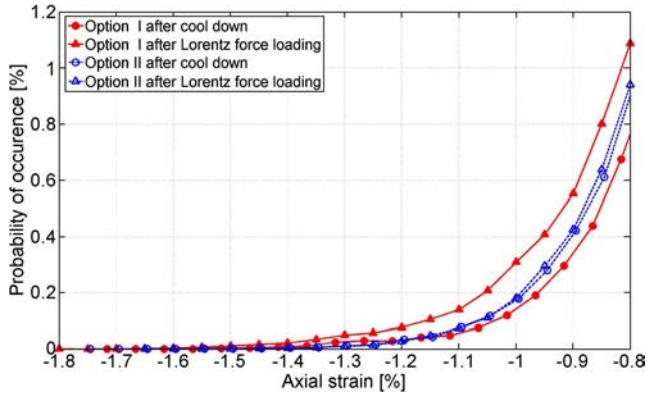

Fig. 6. Tails of the distributions for the compressive part for the two tested samples before and after Lorentz force loading.

Strains exceeding extreme values of $+0.3$ and -0.8% correspond to a reduction of more than 50% of the critical current of common Nb_3Sn strand [18] and should play a role in the degradation of CICC performances.

D. Impact of the Conductor Designs

Some statistical data have been selected from the various distributions: the mean, the percentage of values greater than $+0.3\%$ and the percentages lower than -0.8% (Table II). Regarding these statistics, the two tested cables differ. After loading, the mean of the axial strains increases by 10% in the *Option I* sample but hardly varies in the *Option II* sample. The critical tensions vary by 50% in *Option I* sample but only by 14% in *Option II* sample. The critical compressions change by 78% in *Option I* sample but by only 4.7% in *Option II* sample. At some locations, the entire cross-section of the beam is strained bellow -0.8%. Nevertheless, the proportion of critical events should be related to the length of the cable model and current transfer that may occur in conductor. In that sense, the interaction of the Multifil data with electromagnetic codes may help to assess the conductor electromagnetic performances and bring further information about the optimization of the cable design [19].

V. Conclusion

In the scope of the mechanical characterization of ITER Cable-In-Conduit Conductors, a numerical model is proposed. The simulation of the shaping of the conductor and CICC specific loadings allows the local strains to be assessed along every strand. The presented results highlight the high heterogeneity of strains that develops within the cable where the applied loads are transmitted both into pure compression and bending. The induced critical strains in the tensile and compressive domains may significantly degrade the critical current of the Nb_3Sn strands. The ability of the code to model various designs of cable would eventually help optimize the conductor performances. In particular the interface of the mechanical approach with available electrical model should be carried out.

Acknowledgment

The authors thank CEA Cadarache and ITER IO for their support.

References

[1] N. Mitchell, "Mechanical and magnetic load effects in Nb_3Sn cable-in-conduit conductors," *Cryogenics*, vol. 43, pp. 255–270, 2003.
[2] N. Mitchell, "Operating strain effects in Nb_3Sn cable-in-conduit conductors," *Supercond. Sci. Technol.*, vol. 18, pp. 396–404, 2005.
[3] N. C. van den Eijinden, A. Nijhuis, Y. Ilyin, W. A. J. Wessel, and H. H. J. ten Kate, "Axial tensile stress-strain characterization of ITER model coil type Nb_3Sn strands in TARSIS," *Supercond. Sci. Technol.*, vol. 18, pp. 1523–1532, 2005.
[4] M. C. Jewell, P. J. Lee, and D C. Larbalestier, "The influence of Nb_3Sn strand geometry on filament breakage under bend strain as revealed by metallography," *Supercond. Sci. Technol.*, vol. 16, pp. 1005–1011, 2003.
[5] D. Ciazynski, "Review of Nb_3Sn conductors for ITER," *Fusion Eng. Des.*, vol. 82, pp. 488–497, 2007.
[6] N. Mitchell, "Assessment of conductor degradation in the ITER CS insert coil and implications for the ITER conductors," *Supercond. Sci. Technol.*, vol. 20, pp. 25–34, 2007.
[7] N. Mitchell, "Comparison between prediction and measurement of the superconducting performance of Nb_3Sn cable in conduit conductors with transverse load degradation," *Supercond. Sci. Technol.*, vol. 21, p. 054005, 2008.
[8] A. Nijhuis and A. Y. Ilyin, "Transverse load optimization in Nb_3Sn CICC design; influence of cabling, void fraction and strand stiffness," *Supercond. Sci. Technol.*, vol. 19, pp. 945–962, 2006.
[9] D. Durville, "Numerical simulation of entangled materials mechanical properties," *J. Mater. Sci.*, vol. 40, no. 22, pp. 5941–5948, 2005.
[10] D. Durville, "Contact Modelling in Entangled Fibrous Materials," in *Trends in Computational Contact Mechanics*, ser. Lecture Notes in Applied and Computational Mechanics, G. Zavarise and P. Wriggers, Eds. Berlin, Germany: Springer-Verlag, 2011, vol. 58, pp. 1–22.
[11] H. Bajas, "Numerical simulation of the mechanical behavior of the ITER cable-in-conduit conductors," Ph.D. dissertation, Ecole Centrale de Paris, Paris, France, 2011.
[12] D. P. Boso, M. J. Lefik, and B. A. Schrefler, "Thermal and bending strain on Nb_3Sn strands," *IEEE Trans. Appl. Supercond.*, vol. 16, no. 2, 2006.
[13] D. P. Boso, M. J. Lefik, and B. A. Schrefler, "Thermo-mechanics of the hierarchical structure of ITER superconducting cables," *IEEE Trans. Appl. Supercond.*, vol. 17, no. 2, 2007.
[14] H. Bajas, D. Durville, D. Ciazynski, and A. Devred, "Numerical simulation of the mechanical behaviour of ITER cable-in-conduit conductors," *IEEE Trans. Appl. Supercond.*, vol. 20, no. 3, pp. 1467–1470, 2010.
[15] N. Mitchell, "Finite element simulations of elasto-plastic processes in Nb_3Sn strands," *Cryogenics*, vol. 45, pp. 501–515, 2005.
[16] Y. Miyoshi, E. P. A. van Lanen, and M. M. J. Dhalle, "Distinct voltage-current characteristics of Nb_3Sn strands with dispersed and collective crack distributions," *Supercond. Sci. Technol.*, vol. 22, 2009.
[17] M. C. Jewell, "The effect of strands architecture on the fracture propensity of Nb_3Sn composite wires," Ph.D. dissertation, Univ. Wisconsin, Madison, WI, 2008.
[18] A. Nijhuis, Y. Ilyin, and H. J. G. Krooshoop *et al.*, "ITER Nb_3Sn strand bending and strain test program at the University of Twente," Final Rep. UT-ITER, 2008-2.
[19] A. Torre, H. Bajas, D. Ciazynski, D. Durville, and K. Weiss, "Mechanical-electrical modeling of stretching experiment on 45 Nb_3Sn strands CICCs," *IEEE Trans. Appl. Supercond.*, vol. 21, no. 3, pp. 2042–2045, 2011.
[20] Y. Zhai and M. Bird, "Florida electro-mechanical cable model of Nb_3Sn CICCs for high-field magnet design," *Supercond. Sci. Technol.*, vol. 21, p. 15, 2008.
[21] Y. Zhai, "Electro-mechanical modeling of Nb_3Sn CICC performance degradation due to strand bending and inter-filament current transfer," *Cryogenics*, vol. 50, pp. 149–157, 2010.